Pulmonary Circulation

WILEY

PVRi Pulmonary Circulation Open Access

RESEARCH ARTICLE OPEN ACCESS

Development of a Novel, Pulmonary Endovascular Device to Treat Patients With Pulmonary Hypertension

Karl Vollmers[1] | John Scandurra[1] | Joshua R. Woolley[1] | Guruprasad A. Giridharan[2] | Alexander M. K. Rothman[3] | Marc Pritzker[4] | E. Kenneth Weir[4] | Christian Gerges[5] | Irene Lang[5]

[1]Aria CV, Inc, Saint Paul, Minnesota, USA | [2]University of Louisville, Louisville, Kentucky, USA | [3]The University of Sheffield and Sheffield Teaching Hospitals NHS Foundation Trust, Sheffield, UK | [4]University of Minnesota, Minneapolis, Minnesota, USA | [5]Medical University of Vienna, Vienna, Austria

Correspondence: John Scandurra (jscandurra@ariacv.com)

Received: 1 March 2025 | **Revised:** 8 July 2025 | **Accepted:** 9 July 2025

Funding: Funding for the studies was provided by Aria CV.

ABSTRACT

Pulmonary hypertension (PH) carries a poor prognosis and a high mortality. Loss of pulmonary arterial compliance (PAC) plays a significant role in the development of PH and is an early predictor of mortality. Currently, there are no therapeutic options to overcome the loss of PAC. Aria CV (Saint Paul, MN) has developed a device to augment PAC. The device consists of a 20-cc balloon and anchor that can be implanted in the pulmonary artery using a minimally invasive procedure, a catheter, and a gas reservoir. Computed tomography imaging of 46 patients from the ASPIRE database and cadaver studies ($n = 7$) were used to ascertain device fit and optimize surgical procedure. Aria CV devices ($n = 6$) were tested for simulated use, durability, and PAC augmentation. Animal studies were conducted to demonstrate device safety in the deflated state ($n = 9$), and gas embolism due to simulated balloon rupture ($n = 5$). A chronic bovine model of PH was used to demonstrate PAC augmentation ($n = 3$). Chronic animal studies ($n = 8$, 30-days) were conducted to demonstrate long-term device safety and biocompatibility per ISO 10993 standards. In-silico fit and cadaver studies demonstrated that the device could be successfully implanted in the PA for a wide range of patients. In vitro and bovine models of PH demonstrated that the chronic Aria CV device enhanced PAC by > 0.4 ml/mmHg, which matched the PAC enhancement observed in 28 human patients with a short-term Aria CV device. The device passed all required durability, safety, and biocompatibility testing and is enrolling patients in a Food and Drug Administration (FDA) approved clinical trial (ASPIRE PH, NCT04555161).

1 | Introduction/Background

Pulmonary hypertension (PH) is a progressive disease with a poor long-term prognosis that affects as many as 80 million people worldwide [1]. The median survival for PH is 3–7 years, depending on etiology, severity of disease, and response to therapy [2–4]. PH is classified into 5 groups based on etiology [5]. Although defined by a high pulmonary artery pressure (PAP), a common feature in all PH Groups is increased vascular stiffness (lower pulmonary arterial compliance [PAC]) in the pulmonary arteries with increased pulmonary vascular resistance (PVR) in most cases [6]. These changes result in abnormally high right ventricular (RV) afterload, initiating a series of progressive structural and functional changes culminating in right heart failure (RHF) and death [7].

PH is characterized by an early significant loss of vascular compliance, before a clinically significant increase in PVR [8–11]. The loss of vascular compliance leads to elevated pulmonary artery (PA) pulse pressure, peak systolic pressures, higher pulmonary arterial turbulence, restricted diastolic pulmonary arterial flow, pathologically altered shear stress, loss of normal PA reservoir function, augmented reflectance waves, and stimulation of mechanosensitive receptors, that result in

progressive, pathologic vascular remodeling and elevated PVR [12–16]. While the pulsatile component of RV afterload is thought to constitute approximately 25% of afterload, it has been shown to have a consistent and outsized impact on survival [17, 18].

The increased arterial stiffness associated with loss of PA compliance results in (1) elevated RV afterload early in systole when the RV volume and wall stresses are high, (2) increased RV external work, and (3) alterations in RV pressure volume relationships [19–22]. Reduction in compliance results in the loss of Windkessel reservoir function and acceleration and magnification of PA reflectance waves, which increases RV afterload [23]. Wave reflections reach the native right ventricle when the pulmonic valve is open, resulting in further elevation of the ventricular ejection pressures and RV afterload [24]. Concurrently, elevated RV pressures compromise normal RV systolic coronary perfusion [25]. Unlike left ventricular coronary perfusion, healthy RV coronary perfusion is characterized by perfusion distributed throughout the entire cardiac cycle (systole and diastole) [26]. In PH, coronary flow is impaired, resulting in reduced myocardial oxygen uptake, lower coronary blood flow, reduced oxygen delivery, and functional ischemia. Thus, a reduction in RV systolic coronary perfusion contributes to a significant compromise of RV coronary reserve and the potential for myocardial hypoxia/ischemia in the presence of increased RV afterload [27–29].

In PH, the abnormally elevated RV afterload is comprised of two components: steady state and pulsatile load [8, 30]. Steady state load elevation is due to PVR increase and manifests as an elevated mean PAP Pulsatile load elevation is related to low PAC and results in elevated pulmonary pulse pressure. When the RV ejects into a normally compliant PA, one portion of the ejected blood flows through the pulmonary vasculature during systole and one fraction is temporarily stored due to the elastic deformation of the pulmonary arterial vasculature and is released during diastole. In patients with low pulmonary compliance, a significant amount of flow needs to pass through the pulmonary vasculature during the short systolic ejection phase with minimal diastolic flow due to a reduced storage component [8, 16]. Thus, low pulmonary vascular compliance results in high RV load that must be overcome during ejection.

Higher RV pressures and wall stresses cause ventricular pathologic remodeling ultimately resulting in RV dysfunction [31]. RV function and structure are highly dependent upon normal RV-PA coupling; which is the matching of contractility to afterload [18, 32, 33]. In the setting of increased RV afterload, RV-PA coupling is initially preserved, due to increased RV contractility, hypertrophy and dilatation, resulting in the maintenance of cardiac index, tricuspid annular plane systolic excursion (TAPSE), and right ventricular ejection fraction (RVEF) within a normal range [34].

RV-PA decoupling occurs when RV adaption cannot match the progressively increasing adverse remodeling associated with elevated RV afterload, resulting in RV dysfunction and RHF [35]. RV function is highly correlated with outcomes and RV function is the primary risk factor for mortality in patients with PH [36–39]. Nearly two-thirds of mortality associated with chronic PH has been attributed to RV failure [40]. Elevated systolic ventricular afterload alters RV contraction, resulting in dyssynchrony [41, 42]. RV isovolumetric contraction after aortic valve closure, due to a late leftward shift of the septum, augments dyssynchrony, impairs biventricular filling, and reduces stroke volume and cardiac output [43].

Currently employed pharmacologic options are mostly targeted to Group 1 physiology and predominantly lower PVR. However, research has shown that PVR is only weakly correlated with PH clinical outcomes [44]. Therapeutic options that dominantly target PVR do not address the other fundamental mechanical, functional, and structural aspects associated with PH, including the abnormally elevated pulmonary vascular stiffness (low compliance), adverse RV remodeling and dysfunction. While pharmacologic treatment results in PVR improvements, it does not abrogate progressive clinical deterioration leading to poor prognosis [45–48]. While the loss of compliance has been demonstrated to be an early and progressive predictor of mortality in humans [49, 50], a therapeutic option to specifically target the loss of PA compliance does not exist. To overcome this limitation, Aria CV Inc (St. Paul, MN) developed a chronic device that augments PA compliance and shields the RV from the increased pulsatile RV afterload. Previously, Aria CV had developed and implanted a short-term device in a human clinical trial. This manuscript presents the development and testing of the second-generation, chronic Aria CV device resulting in an FDA approved clinical study.

2 | Methods

2.1 | Device, Implantation, and Method of Action

The Aria CV device is a totally implanted, long-term, PH system that requires no external connection or power source. The device consists of a 20cc gas-filled balloon positioned in the main PA, a nitinol anchor located in the left PA, an implantable, subcutaneous gas-filled reservoir, and a 12 F catheter that connects the balloon to the gas reservoir and enables rapid flow of gas between them in response to changes in intravascular pressure during systole and diastole. (Figure 1). The balloon is designed to be non-obstructive as the diameter of the balloon is significantly smaller than the diameter of the main PA in patients with PH [51].

The device is implanted using a minimally invasive surgical technique. A small cut-down incision is made into the subclavian vein and a 22 F introducer is inserted. A standard guidewire is inserted through the subclavian vein and advanced into the left PA. A 20 Fr delivery sheath with a hemostatic valve is advanced to the main PA. The 12 Fr catheter with the attached balloon and nitinol anchor is advanced through the sheath. The sheath and introducer are removed, and hemostasis is achieved with purse-string sutures. The extravascular portion of the catheter is then tunneled subcutaneously to the abdomen. The gas reservoir is implanted subcutaneously on the anterior abdominal wall, and the tunneled catheter is connected. The device is then filled via needle puncture into the reservoir fill port with a proprietary mix of gases (primarily N_2, O_2, CO_2) that has low permeability through the balloon. Any gas that diffuses

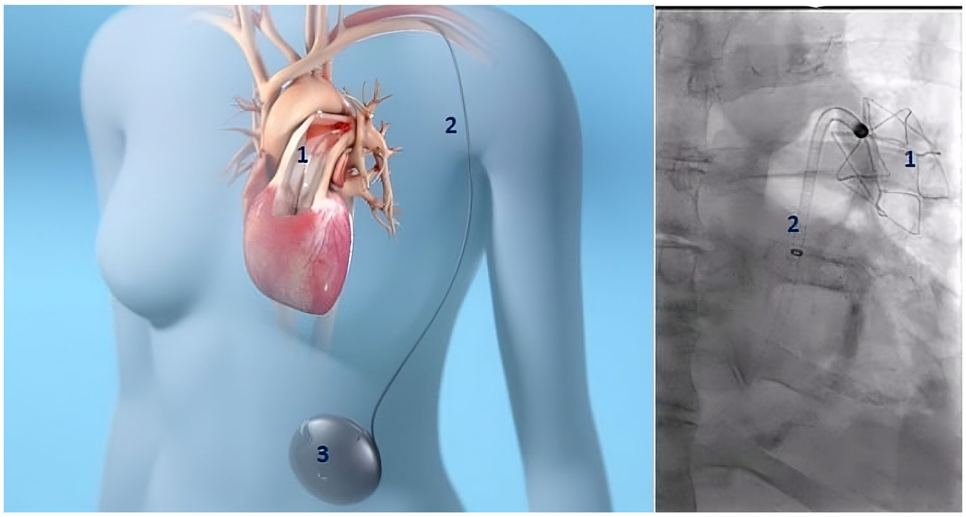

FIGURE 1 | Left—Aria CV device pulmonary endovascular device consisting of a (1) balloon in the pulmonary artery and nitinol anchor in the left main branch y, (2) 12 Fr catheter, and (3) a gas reservoir. Right—Aria CV pulmonary endovascular device in situ.

through the polymer membranes is absorbed into the blood and exits through the lungs. The balloon catheter is designed to be detachable from the nitinol anchor if the device needs to be explanted after anchor ingrowth.

During systole, as the pressure rises in the PA, gas in the balloon is compressed and gas moves from the balloon through the conduit and into the reservoir. The progressive decrease in the volume of the balloon ensures the balloon is non-obstructive and makes space in the proximal PA for the incoming stroke volume of blood, like a healthy compliant PA that would stretch to make room for the RV stroke volume. The hemodynamic effect is to decrease systolic pressure and workload on the RV which can now eject more blood at lower pressure. During diastole, the pressure gradient between the reservoir and the pulmonary vasculature is reversed and the gas returns from the reservoir to fill the balloon. The diastolic increase in the volume of the balloon pushes blood into the distal pulmonary capillary bed augmenting diastolic PA flow. Thus, the Aria CV device compensates for the lack of compliance in the pulmonary arterial vasculature. The PA systolic pressure is reduced, and the diastolic pressure increases, resulting in a drop in PA pulse pressure.

2.2 | Testing

The Aria CV device underwent extensive in silico, cadaver, in vitro, and acute and chronic animal studies to demonstrate anatomic fit, device durability, procedural and device safety, device efficacy, and to optimize the implantation procedure. These studies are presented next.

2.2.1 | In Silico Fit Study

Anatomic data were extracted from clinically obtained computed tomography (CT) scans in PH patients of different size and gender ($n = 46$, Male = 26, 64.3 ± 13.4 years) from the ASPIRE registry [52]. The ASPIRE Registry includes deidentified data on consecutive patients undergoing investigation for suspected PH at the Sheffield Pulmonary Vascular Disease Unit. Ethical approval was granted by the Institutional Review Board and approved by the National Research Ethics Service (16/YH/0352 subsequently 22/EE/0011). The patient cohort included WHO Group 1 ($n = 26$), Group 2 ($n = 4$), and Group 3 ($n = 5$) patients. Mean PAP in the patient cohort was 46.9 ± 12.8 mmHg. PA left branch diameter and length from the pulmonary valve to the anchor location measurements were recorded because these measurements are critical to Aria CV device implant.

2.2.2 | Cadaver Study

A cadaver study ($n = 7$) was conducted to evaluate and refine the surgical technique, evaluate potential forces generated during torso and arm movements that might affect the device catheter, and to optimize the tunneling pathway to minimize external forces or catheter deformation. The arm and torso movements included simulated shoulder flexion/extension (~ −30 to −180°), shoulder adduction/abduction (−180°), and torso rotation (~ 0–60°). Once the implant procedure was optimized, studies were conducted to evaluate ease of implant and quantify the forces due to torso and arm movements on the device.

2.2.3 | In Vitro Studies

The Aria CV balloon, anchor, and device catheter ($n = 6$) were tested for simulated use, compliance enhancement, anchoring forces, durability, and compliance augmentation after gamma sterilization.

2.2.3.1 | Simulated Use. In the simulated use testing, the sterilized Aria CV device ($n = 6$) was delivered in a 3D anatomical model of the vasculature (derived from previously obtained CT scans) from the subclavian vein to the PA in a body temperature water bath. The Aria CV delivery catheter was

advanced over the guidewire to the PA and the balloon catheter and anchor deployed. The system flexibility, kink resistance, pushability, and trackability were examined. The implant positioning, deployment, recapture and redeployment and delivery system withdrawal were also assessed.

2.2.3.2 | Pulse Duplicator for Compliance Testing. The pulse duplicator is a modified valve tester and consists of a mock right atrium, right ventricle, pulmonary valve, PA, and adjustable PA and lung compliances and resistances (Figure 2). The pulse duplicator was instrumented with pressure and flow sensors integrated with a custom data acquisition system. The Aria CV device was implanted in the mock PA. The pulse duplicator was filled with water and was tuned to mimic the PA hemodynamics and compliance of patients with PH. PA hemodynamic measurements were obtained during baseline with the device deactivated (gas was evacuated from the device, reservoir pressure at ~ mean pulmonary arterial pressure of the system) and with the device activated (gas cycling back and forth). PA compliance was calculated based on hemodynamic measurements before and after device activation.

2.2.3.3 | Anchoring Forces. The nitinol anchor was crimped down in the loader and delivered through the 0.250" guiding catheter. A radial expansion force gauge (RX650, Machine Solutions Inc.) with an encoder for diameter accuracy was used for radial force measurement. The radial forces were measured at 16 mm and 22 mm (range of pulmonary vessel diameters where the device was anchored) in 37°C saline. The passing criterion was an anchoring force between 5 N to 9 N, a range shown not to cause damage in normotensive sheep pulmonary arteries.

2.2.3.4 | Durability Tests. Durability tests were conducted following ISO 5840 standards and in consultation with the Food and Drug Administration for the early feasibility study.

2.2.3.4.1 | Balloon. The balloon durability was tested in modified valve durability test units. The balloon displacement volume was representative of physiologic displacement. The balloon was frequently subjected to worst-case fatigue conditions and allowed to reach a fully depleted state during simulated end-systole. An additional 10 million cycles were conducted to simulate an overfilled balloon. The balloon was evaluated for the ability to disconnect from the anchor, balloon structural integrity, and helium permeance rate at the end of the test. Additionally, the ability of the balloon to add compliance (≥ 0.4 ml/mmHg) was evaluated in a hydrodynamic pulse duplicator before and after durability testing.

2.2.3.4.2 | Anchor Deflection Testing. The loading profile and x-y displacement of the anchor was 0.25 ± 0.1 mm and was tested at 25 Hz per American Society for Testing and Materials (ASTM) standard (Figure 3). Following the completion, the x–y displacement was increased to a worst-case

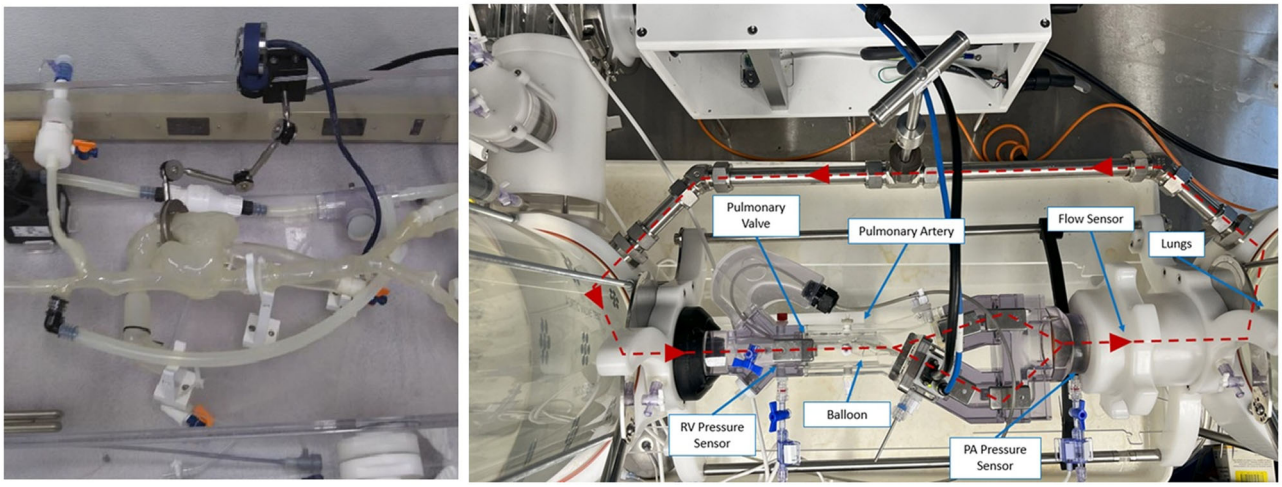

FIGURE 2 | Left—Anatomical model used for simulated use testing, Right—Pulse duplicator system for compliance testing.

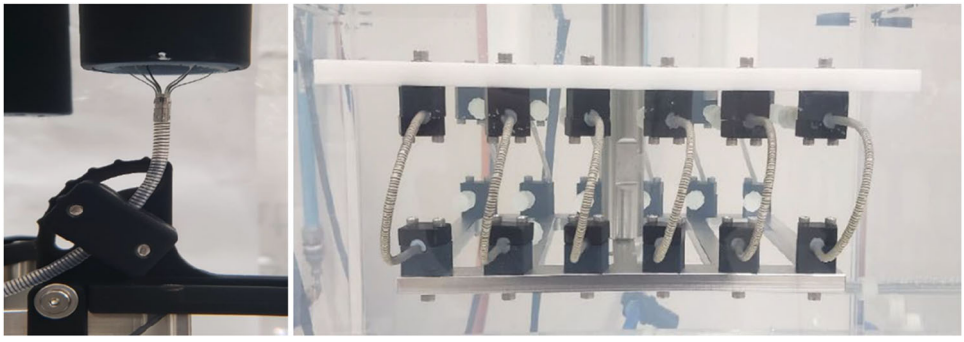

FIGURE 3 | Left - Axial anchor deflection testing, Right - Catheter bend testing.

0.68 ± 0.1 mm displacement and tested for 10 million additional cycles at 72 beats per minute. The anchor motion was recorded via high-speed camera and the deflection was measured in x-direction (lateral movement), y-direction (axial movement), and theta (rotational movement). The anchor was inspected visually for structural integrity, and anchor disconnection torque was measured at the end of the test.

2.2.3.4.3 | Catheter Bend Testing. The 12 Fr balloon catheter was subjected to ± 0.75 mm sinusoidal alternating displacement in 37°C saline at 30 Hz. The catheter was held at 57 mm vertical offset and 26 angular offset to mimic the in vivo positioning in a patient (Figure 3). The ± 0.75 mm cyclic displacement is representative of the intravascular motion of the catheter induced by the cardiac cycle to demonstrate long term durability of the implant. The catheter was evaluated for structural integrity at the end of the test.

2.3 | Animal Studies

Bovine and ovine animal models were utilized to demonstrate device efficacy and safety. All animal studies were approved by the appropriate Institutional Animal Care and Use Committees (IACUC).

2.3.1 | Efficacy Testing Using Hypoxic Bovine Model

Holstein ($n = 6$) and Angus ($n = 3$) calves, approximately 3 weeks of age were acclimated at ambient conditions for at least a week. Baseline measurements including right heart catheterization, transthoracic cardiac echo, and blood draws were collected. To replicate the naturally occurring high altitude "brisket" disease, the animals were housed in normobaric hypoxic stalls that simulated oxygen partial pressures equivalent to altitudes of up to 18,000 feet (Figure 4). The animals were exposed to gradually increasing altitudes (levels of hypoxia), in the chambers to simulate 12,000 feet of altitude at 90 days. Right heart catheterization, blood draws, and transthoracic cardiac echoes were performed monthly unless the observational status of the calves changed and assessment was deemed necessary. After reaching a state of dilated RV failure, the animals were anesthetized, and the Aria CV device implanted in the main PA. At the start of the procedure, a standard right heart catheterization was performed at baseline using a 7Fr. Swan Ganz catheter and thermodilution using jugular venous access. During baseline and device activation conditions, cardiac output (CO) was measured in quintuplicate by thermodilution and the results averaged. The clinically simplified stroke volume (SV)/pulse pressure (PP) formula was used to calculate PAC where SV was determined from CO/heart rate (HR). PVR was calculated using the formula: PVR = (mPAP − Pulmonary Capillary Wedge Pressure [PCWP])/CO. The PAP waveform was averaged to get the mPAP. At the end of the procedure, the animal was electively euthanized under anesthesia. A paired, single tailed T-test was used to calculate statistically significant differences.

2.3.2 | Deflated Device Safety Testing

To evaluate the safety of the device when the Aria CV balloon was deflated, which is the worst-case scenario for thrombus formation, a chronic animal study was conducted in a healthy ovine animal model ($n = 9$, 5 females, 4 males). The animal was anticoagulated using heparin to maintain an ACT of 180–400 s during implant procedure. Vascular access was through the right internal jugular and the device was implanted in the PA. The catheter was tunneled to the reservoir that was placed subcutaneously on the dorsal flank of the animal. The gas mixture was evacuated from the reservoir to a pressure of − 200 mmHg, ensuring the balloon was maximally deflated, resulting in the worst-case for sharp creases and thrombosis. The animals were anticoagulated with enoxaparin (2 mg/kg, twice daily), and monitored for clinically significant adverse events during the study period. Bloodwork (CBC, serum chemistry, and coagulation) was collected for clinical pathology assessments at baseline (before treatment) as well as on the day of termination. Animal weights and body condition scores (BCS) were obtained at baseline (before treatment) as well as on the day of termination. At the end of the study period, the animals were heparinized (20,000 IU), euthanized, and gross necropsy was performed by a board-certified veterinary pathologist. The entire device pathway was examined, including the subcutaneous pocket, subcutaneous connective tissue, right jugular vein, superior vena cava, right heart, tricuspid and pulmonic valves, pulmonary trunk and the left PA. The device, including anchor, balloon, and the catheter was examined for thrombus formation and assigned a quantitative clot score. End organs, including lungs, were examined for thrombus and lesions.

FIGURE 4 | Normobaric hypoxic stalls were used create a bovine model of pulmonary hypertension.

2.3.3 | Gas Safety Testing

To evaluate the safety of the Aria CV device in the unlikely event that the gas from the device is released into the blood due to balloon rupture, 24 ml (representative of full balloon volume) of the proprietary gas was injected into the left PA in a sheep model ($n = 5$). Hemodynamics (pulmonary and systemic blood pressures and CO), blood oxygenation and visual observation of the gas embolus and blood flow on contrast fluoroscopy were monitored until the gas embolus was completely reabsorbed and the affected lung returned to baseline. Specifically, measurements were performed at baseline, immediately after gas bolus injection, 10 min after bolus, and every 30 min after the bolus injection until the emboli were no longer visible and blood flow was fully restored as observed on contrast fluoroscopy. Visual analysis of the angiograms and comparison to baseline were made to check for (a) visibly blocked vessels (vessels visible at baseline that don't fully fill with contrast after gas embolism) and (b) contrast blush of tissue at the margins of the lung downstream of the gas emboli. After euthanasia, a targeted necropsy with histopathology of the lungs was performed to assess for evidence of acute lung injury.

2.3.4 | Chronic Animal Testing

The chronic safety of the Aria CV device was evaluated in a 60-day animal study in a healthy ovine model ($n = 8$). During device implantation, the delivery system and placement of the device was evaluated per ISO 10993-4. The reservoir was implanted at the base of the neck. After device and reservoir implant, each animal was recovered and monitored for adverse events. After elective euthanasia, gross necropsy was performed and the device, device pathway, and end-organs were examined for thrombus and structural integrity. Histopathological analyzes were performed per ISO 10993-11 for chronic and sub-chronic toxicity.

3 | Results

Anatomic fit, durability, and procedural and device safety and efficacy were successfully demonstrated. Details of these results are presented below:

3.1 | In Silico Anatomic Fit and Cadaver Testing

In the 46 PH patient CT scans reviewed, the diameters of the left branch and main PA were characterized. These studies demonstrated that the Aria CV device can be anchored in a target landing zone diameter in the left main branch of the PA. The implant procedure and tunneling of the catheter to the reservoir were optimized in the cadaver study. Cadaver study results demonstrated that the forces due to arm and torso movements were less than 1 pound-force (lbf) and within the device specifications (3.4 lbf).

3.1.1 | In Vitro Testing

The simulated use test passed all specifications with successful delivery, recapture and redeployment of all 6 devices. The pulse duplicator compliance tests demonstrated that the Aria CV device activation increased PA compliance by 0.43 ± 0.01 ml/mmHg. The anchoring force for the nitinol anchor was 8.43 ± 0.11 N (8.23–8.59 N) at 16 mm diameter and 8.00 ± 0.29 N (7.60–8.45 N) at a diameter of 22 mm. All Aria CV device components passed durability testing. The balloon could be disconnected from the anchor at the end of the durability test, demonstrating the ability to explant the balloon, if needed, after chronic implant. After the durability test, the balloon increased pulmonary compliance by 0.43 ± 0.01 ml/mmHg (range = 0.40 – 0.44 ml/mmHg). The helium permeance rate after durability testing was $1.33 \times 10^{-4} \pm 9.36 \times 10^{-6}$ ml/s (Range = $1.19 - 1.45 \times 10^{-4}$ ml/s), passing the helium permeance rate specifications.

3.2 | Animal Studies

3.2.1 | Hypoxic Model Efficacy Testing

Eight out of nine animals exhibited progressive development of PH and RHF with graded exposure to normobaric hypoxia. One animal died during model development and one animal had a cardiac arrest during induction of anesthesia, before device placement. The Aria CV device was successfully implanted in the six remaining animals. Three of the six animals developed other physiologic complications due to model development (tricuspid regurgitation, hemodynamic instability, normalization of pulmonary pressure and LV function) that did not allow complete collection of efficacy data.

Paired hemodynamic data including right heart catheter and wedge pressure were measured at baseline and device activation were obtained in the three remaining calves with PAH. Despite the tested calves having a higher PA compliance than humans with PH, all three animals demonstrated an increase in pulmonary compliance with device activation. Improvement in CO and RV stroke volume suggest an improvement in RV function upon device activation, resulting in an increase in mean and systolic PAP. Despite an increase in CO, there was a reduction in PA pulse pressure (Table 1). Significantly, echocardiography data demonstrated PA compliance enhancement due to Aria CV device activation, augmented diastolic PA flow and preserved systolic flow, resulting in a higher stroke volume and CO (Figure 5).

3.2.2 | Deflated Device Thrombogenicity Testing

Seven out of nine animals were successfully implanted with the Aria CV device. Two animals were excluded from the study due to non-device related adverse events (cardiac arrhythmia and anesthesia intolerance). Animals were electively euthanized at a planned endpoint of 15 days ($n = 3$) and 30-days ($n = 4$). No clinically significant adverse events such as thrombosis, pulmonary embolism/infarction, or death related to the Aria CV device were observed.

3.2.3 | Gas Safety Testing

The gas was absorbed in all 5 animals within 150 min. The blood oxygen saturation SPO_2 measurements were 96% or

TABLE 1 | Data demonstrating the hemodynamic changes due to Aria CV device activation (device status on) compared to baseline (device status off).

	Calf 1		Calf 2		Calf 3			
Device status	**Off**	**On**	**Off**	**On**	**Off**	**On**	***p*-value**	
sPAP	38.2	38.5	39.3	40.7	44.5	44.2	0.224	
dPAP	20.9	23.9	19.0	21.3	29.7	31.5	0.010	
mPAP	27.6	29.9	27.8	30.6	35.2	35.5	0.071	
PVR	2.5	2.4	2.0	2.2	2.8	2.8	0.371	
PA PP	17.5	14.7	20.3	19.4	14.8	12.7	0.037	
CO	6.3	7.5	7.7	8.3	7.5	7.8	0.059	
HR	72	72	89	90	87	86	0.500	
PAC	5.0	7.0	4.3	4.8	5.9	7.1	0.052	**Average**
PAC change	**+2.1**		**+0.5**		**+1.2**			**+1.3**
CO change	**+1.2**		**+0.6**		**+0.3**			**+0.7**
PP change	**−2.8**		**−0.9**		**−2.1**			**−1.9**

Abbreviations: CO, cardiac output; dPAP, diastolic pulmonary artery pressure; HR, heart rate; mPAP, mean pulmonary artery pressure; PA PP, pulmonary artery pulse pressure; PAC, pulmonary artery compliance; PVR, pulmonary vascular resistance; sPAP, systolic pulmonary artery pressure.

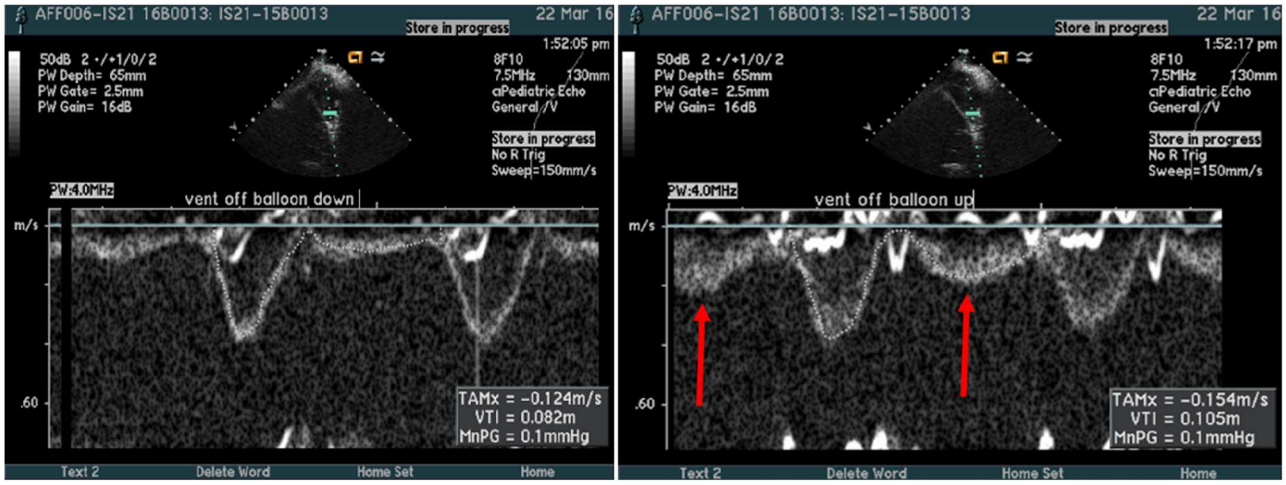

FIGURE 5 | Sample echocardiography animal data showed minimal pulmonary artery (PA) diastolic flow without device activation (left), and with Aria CV device activation augmented diastolic pulmonary artery flow (right, arrow). peak diastolic velocity in the PA with the device off was 0.08 ± 0.02 m/s and the velocity time integral (VTI) over the cardiac cycle was 0.082 m (left). With the device activated (right), the peak diastolic velocity and VTI increased significantly to 0.22 ± 0.02 m/s and 0.105 m, respectively.

higher in all animals throughout the study. The CO increased briefly after gas bolus injection and returned to baseline values within 60 min and remained stable until euthanasia. There were no gross or microscopic pathology findings consistent with lung injury, suggesting that all the gas was absorbed and perfusion to the tissues was not affected by the injection of gas. These results demonstrate the safety of the Aria CV device even during a simulated balloon failure.

3.2.4 | Chronic Animal Testing

The Aria CV device was successfully implanted in all 8 GLP ovine animals. The system passed the ISO 10993 tests for implantation, thrombogenicity, and toxicity. Necropsy findings were unremarkable (Figure 6) and no device related adverse events were observed in any of the animals after 60-days of implant.

4 | Discussion

The in silico, cadaver, bench, animal, and clinical studies consistently demonstrated the ability of the Aria CV device to increase pulmonary vascular compliance by approximately 0.4 mmHg/ml, augment cardiac output and stroke volume, and narrow PA pulse pressure as designed and expected.

In a seminal manuscript examining the correlation of varying degrees of baseline compliance in a series of PAH patients in the lowest pulmonary vascular capacitance quartile reported a 4-year mortality of 61% compared to 15% mortality in the next

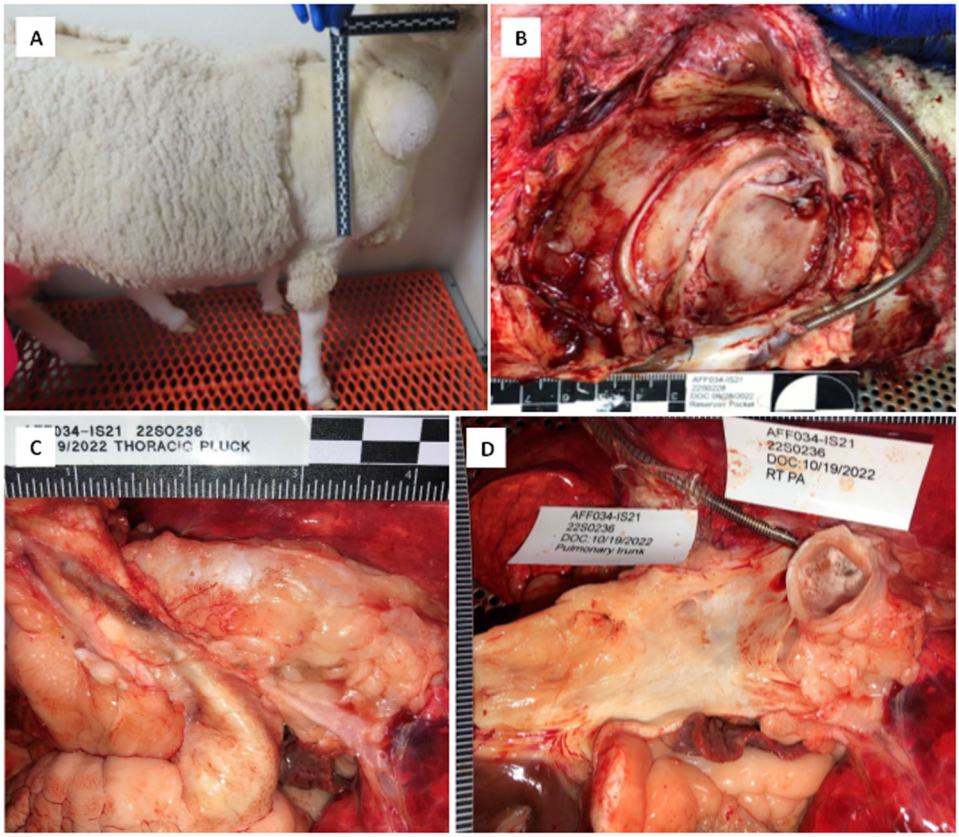

FIGURE 6 | (A) Device implanted in a sheep for 60-days. (B) Reservoir pocket, (C) device in-situ, and (D) pulmonary artery after euthanasia was unremarkable.

lowest (second) quartile [53]. Comparing the results in compliance changes obtained with the Aria CV device activation, the 0.4 mmHg/ml change could theoretically shift patients from the lowest compliance quartile to the second quartile.

Higher vascular compliance is strongly related to lower mortality risk [53]. Thus, the long-term improvement in pulmonary compliance due to Aria CV implantation, though mechanical, is hypothesized to improve RV energetics by reducing peak pulmonary pressures. The energy expended by the right ventricle to eject blood is inversely proportional to pulmonary vascular compliance [54]. During ejection, while some of the ejected stroke volume flows through the vasculature, a large portion of the ejected blood is temporarily stored in the pulmonary vasculature during the ejection phase. Significantly, the stored blood, enabled by vessel elasticity, results in diastolic PA flow, distributing the ventricular outflow over the entire cardiac cycle and lowering ventricular energy expenditure [55].

Aria CV device implantation in calves resulted in a reduction of PA systolic and pulse pressures, RV systolic pressures, and an improvement in PAC and CO. These hemodynamic benefits were observed clinically in humans with a short-term Aria CV device that had a non-anchored 20 ml balloon, and an external reservoir. Briefly, the short-term Aria CV device was implanted in Group 1 ($n = 10$), Group 2 ($n = 8$), and Group 3 ($n = 10$) PH patients [56, 57]. Device activation in Group 1 patients resulted in reduction of pulse pressures (47.6 ± 12.1 mmHg to 44.1 ± 11.6 mmHg), augmentation of cardiac output (6.8 ± 1.7 l/min to 7.5 ± 2.2 l/min), PAC (2.1 ± 1.0 to 2.5 ± 1.2), and end-systolic elastance (E_{es})/effective arterial elastance (E_a; 1.01 ± 0.25 to 1.27 ± 0.21). Device activation in Group 2 patients resulted in statistically significant reductions in PA pulse pressure (5.6 ± 4.2 mmHg), augmentation of PAC (0.4 ± 0.2 ml/mmHg), and increased right ventricular-to-pulmonary vascular (RV-PV) coupling by 0.24 ± 0.18. In Group 3 patients, device activation resulted statistically significant reduction of PA pulse pressures (4.2 ± 2.2 mmHg), compliance (0.4 ± 0.3 ml/mmHg), and increased RV-PV coupling by 0.11 ± 0.07. These results demonstrate the clinical efficacy of the Aria CV device. Increased pulmonary vascular compliance due to device implant may delay wave reflections, lower ejection pressures and afterload, further improving RV energetics and protecting the RV from the deleterious effects of higher pulsatile load in PH.

Aria CV device activation and the concomitant increase in pulmonary vascular compliance resulted in an immediate improvement in stroke volume dependent cardiac output and function (without increasing left ventricular end diastolic pressures), demonstrating that the Aria CV device is non-obstructive in the main PA. The Aria CV device augments PAC using mechanical means, and while the mechanisms for the immediate hemodynamic improvements are not fully known in this study, hypothesized factors potentially associated with these immediate hemodynamic improvements may include—(1) augmentation of diastolic PA flows (Figure 5), (2) improving the timing and magnitude of RV ejection flow, contraction and reversing the ventricular dyssynchony, (3) improved RV-vascular coupling, (4) reduction of systemic and pulmonary

TABLE 2 | Comparison of hemodynamic improvement between Aria CV device and commonly used cardiac assist technologies.

Device	Cardiac index Improvement ($L/min/m^2$)	Cardiac output improvement (L/min)
Aria CV	**0.3–0.9** [53, 54]	**0.6–1.8** [53, 54]
IABP	−0.3–1.2 [58]	0.5–1.0 [59–61]
BiV pacing/CRT	0.1–0.8 [62] (up to 30% non-responders [63, 64])	0.1–1.2 [65]

venous congestion, (5) restoration of interventricular septal geometry and improved septal contribution to ejection, (6) improved systolic RV coronary perfusion and lower ventricular energy expenditure and (7) improvement in intra- and interventricular dyssynchrony.

Significantly, the improvement in CO was dynamic, with more pronounced effects during exercise with the Aria CV device, potentially increasing exercise tolerance and quality of life in patients with PH [56]. The magnitude of CO improvement with Aria CV device implant was similar in magnitude to the CO changes observed in intra-aortic balloon pumping and biventricular pacing in patients with left ventricular failure (Table 2) [58–65]. Significantly, in a small clinical trial for patients with PH, biventricular pacing reduced cardiac output in 4 out of 6 patients [65].

The loss of compliance, and increase in vascular resistance, ventricular and vascular pressures, and ventricular afterload resulting in RV failure and mortality is a common feature in PH. During PH, mechanosensation and mechanotransduction of the non-physiologic pulmonary arterial pulse pressures, arterial shear, and ventricular wall stress have been implicated in triggering the remodeling of the pulmonary vasculature and right ventricle, which contributes to the progression of disease in a positive feedback loop [5, 15, 66–69]. Mechanotransduction, sensed by cell surface, cytoplasmic and extracellular matrix (ECM) receptors induce gene transcription and biological signals that drive vascular remodeling, including hypertrophy, hyperplasia, apoptosis, and ECM synthesis and degradation in attempts to maintain vascular and regional pulmonary homeostasis. The large proximal arteries and the small distal arteries and capillaries are in a dynamic, feed forward dialog that result in continuing loss of vascular compliance and pathologic molecular activation resulting in continuing adverse ventriculo-vascular remodeling. Compliance alteration in the proximal pulmonary vasculature amplifies pulse-wave transmission to the distal pulmonary arteries, and can result in inflammation, pathologic shear stress, endothelial injury, and smooth muscle remodeling. Distal pulmonary vascular compliance changes associated with muscularization increase the mean vascular pressures and result in continuing large vessel remodeling including wall thickening, dilation, and alterations in ECM [70–72]. The addition of compliance due to the Aria CV device implant, and the resulting reduction of these abnormal biomechanical signals may potentially induce reverse remodeling [73] by favorably altering gene activation and transcription in myocardial and vascular cells. RV and vascular reverse remodeling attributed to reduced systemic and pulmonary congestion and normalization of vascular pressures has been previously reported with lung transplantation [74, 75] and left sided mechanical support in patients with biventricular failure [76–78].

In summary, the Aria CV device is designed to be a chronic intravascular device to enhance pulmonary vascular compliance. Compliance enhancement with Aria CV device therapy is synergistic with drug therapy that focuses on PVR. In vitro and animal studies have demonstrated the safety of chronic device implantation and the feasibility of the device to augment the pulmonary vascular compliance, reduce RV afterload and pulmonary pressures chronically. These studies have resulted in the Food and Drug Administration (FDA) approval of a 30-subject clinical trial for Groups 1, 2 and 3 PH with RV dysfunction.

5 | Limitations

There was variability in the development of PH in the hypoxia calf study and mortality was high. The pulmonary compliance in calves is higher than in humans with PH. Device implant was through the right jugular vein in the animal models to accommodate the anatomy of the animal. In vitro testing is not capable of replicating all physiological responses. Despite these limitations, extensive testing of the Aria CV device through multiple models per FDA and ISO standards successfully demonstrated safety and efficacy, resulting in FDA approval of a clinical trial.

Author Contributions

Karl Vollmers: data generation, data analysis, writing – review and editing. **John Scandurra:** funding acquisition, writing – original draft. **Joshua R. Woolley:** conceptualization, writing – original draft **Guruprasad A. Giridharan:** conceptualization, and writing – original draft. **Alexander M.K. Rothman:** data acquisition, review, editing. **Marc Pritzker:** writing – review and editing. E. **Kenneth Weir:** writing – review and editing. **Christian Gerges:** writing – review and editing. **Irene Lang:** conceptualization, writing – review and editing.

Acknowledgments

The authors would like to thank the Sheffield ASPIRE consortium for providing access to the registry data for virtual anatomic fit studies. ASPIRE registry is supported by the National Institute for Health and Care Research (NIHR) Sheffield Biomedical Research Center (NIHR203321). Funding for the studies was provided by Aria CV.

Ethics Statement

All animal studies were approved by the appropriate Institutional Animal Care and Use Committees (IACUC). Ethical approval for the ASPIRE registry for human imaging data was granted by the Institutional Review Board and approved by the National Research Ethics Service (16/YH/0352 subsequently 22/EE/0011).

Conflicts of Interest

Karl Vollmers: Employee of Aria CV. John Scandurra: Employee of Aria CV. Joshua R. Woolley: Employee of Aria CV. Guruprasad A.

Giridharan: Employee of the University of Louisville, Consultant. Alexander Rothman: Employee of University of Sheffield. Marc Pritzker: Employee of the University of Minnesota, Consultant. E. Kenneth Weir: Employee of the University of Minnesota, Consultant. Christian Gerges: Employee of Medical University of Vienna. Irene Lang: Employee of Medical University of Vienna.

References

1. M. M. Hoeper, M. Humbert, R. Souza, et al., "A Global View of Pulmonary Hypertension," *Lancet Respiratory Medicine* 4 (2016): 306–322, https://doi.org/10.1016/S2213-2600(15)00543-3.

2. K. M. Olsson, M. Delcroix, H. A. Ghofrani, et al., "Anticoagulation and Survival in Pulmonary Arterial Hypertension," *Circulation* 129 (2014): 57–65, https://doi.org/10.1161/CIRCULATIONAHA.113.004526.

3. H. Gall, J. F. Felix, F. K. Schneck, et al., "The Giessen Pulmonary Hypertension Registry: Survival in Pulmonary Hypertension Subgroups," *Journal of Heart and Lung Transplantation* 36 (2017): 957–967, https://doi.org/10.1016/j.healun.2017.02.016.

4. V. V. McLaughlin, K. W. Presberg, R. L. Doyle, et al., "Prognosis of Pulmonary Arterial Hypertension," *Chest* 126 (2004): 78S–92S, https://doi.org/10.1378/chest.126.1_suppl.78S.

5. G. Simonneau, I. M. Robbins, M. Beghetti, et al., "Updated Clinical Classification of Pulmonary Hypertension," *Journal of the American College of Cardiology* 54 (2009): S43–S54, https://doi.org/10.1016/j.jacc.2009.04.012.

6. Z. Wang and N. C. Chesler, "Pulmonary Vascular Wall Stiffness: An Important Contributor to the Increased Right Ventricular Afterload With Pulmonary Hypertension," *Pulmonary Circulation* 1 (2011): 212–223, https://doi.org/10.4103/2045-8932.83453.

7. G. R. Stevens, A. Garcia-Alvarez, S. Sahni, M. J. Garcia, V. Fuster, and J. Sanz, "RV Dysfunction in Pulmonary Hypertension is Independently Related to Pulmonary Artery Stiffness," *JACC: Cardiovascular Imaging* 5 (2012): 378–387, https://doi.org/10.1016/j.jcmg.2011.11.020.

8. T. Thenappan, K. W. Prins, M. R. Pritzker, J. Scandurra, K. Volmers, and E. K. Weir, "The Critical Role of Pulmonary Arterial Compliance in Pulmonary Hypertension," *Annals of the American Thoracic Society* 13 (2016): 276–284, https://doi.org/10.1513/AnnalsATS.201509-599FR.

9. J. Sanz, M. Kariisa, S. Dellegrottaglie, et al., "Evaluation of Pulmonary Artery Stiffness in Pulmonary Hypertension With Cardiac Magnetic Resonance," *JACC: Cardiovascular Imaging* 2 (2009): 286–295, https://doi.org/10.1016/j.jcmg.2008.08.007.

10. W. Tan, K. Madhavan, K. S. Hunter, D. Park, and K. R. Stenmark, "Vascular Stiffening in Pulmonary Hypertension: Cause or Consequence? (2013 Grover Conference Series)," *Pulmonary Circulation* 4 (2014): 560–580, https://doi.org/10.1086/677370.

11. B. M. Kaess, J. Rong, M. G. Larson, et al., "Aortic Stiffness, Blood Pressure Progression, and Incident Hypertension," *Journal of the American Medical Association* 308 (2012): 875, https://doi.org/10.1001/2012.jama.10503.

12. G. Reiter, U. Reiter, G. Kovacs, et al., "Magnetic Resonance–Derived 3-Dimensional Blood Flow Patterns in the Main Pulmonary Artery as a Marker of Pulmonary Hypertension and a Measure of Elevated Mean Pulmonary Arterial Pressure," *Circulation: Cardiovascular Imaging* 1 (2008): 23–30, https://doi.org/10.1161/CIRCIMAGING.108.780247.

13. J. T. Marcus, C. T.-J. Gan, J. J. M. Zwanenburg, et al., "Interventricular Mechanical Asynchrony in Pulmonary Arterial Hypertension," *Journal of the American College of Cardiology* 51 (2008): 750–757, https://doi.org/10.1016/j.jacc.2007.10.041.

14. G.-J. Mauritz, J. T. Marcus, N. Westerhof, P. E. Postmus, and A. Vonk-Noordegraaf, "Prolonged Right Ventricular Post-Systolic Isovolumic Period in Pulmonary Arterial Hypertension is not a Reflection of Diastolic Dysfunction," *Heart* 97 (2011): 473–478, https://doi.org/10.1136/hrt.2010.193375.

15. S. Barbeau, G. Gilbert, G. Cardouat, et al., "Mechanosensitivity in Pulmonary Circulation: Pathophysiological Relevance of Stretch-Activated Channels in Pulmonary Hypertension," *Biomolecules* 11 (2021): 1389, https://doi.org/10.3390/biom11091389.

16. J. L. Cavalcante, J. A. C. Lima, A. Redheuil, and M. H. Al-Mallah, "Aortic Stiffness," *Journal of the American College of Cardiology* 57 (2011): 1511–1522, https://doi.org/10.1016/j.jacc.2010.12.017.

17. N. Saouti, N. Westerhof, F. Helderman, et al., "Right Ventricular Oscillatory Power is a Constant Fraction of Total Power Irrespective of Pulmonary Artery Pressure," *American Journal of Respiratory and Critical Care Medicine* 182 (2010): 1315–1320, https://doi.org/10.1164/rccm.200910-1643OC.

18. A. Vonk Noordegraaf, B. E. Westerhof, and N. Westerhof, "The Relationship Between the Right Ventricle and its Load in Pulmonary Hypertension," *Journal of the American College of Cardiology* 69 (2017): 236–243, https://doi.org/10.1016/j.jacc.2016.10.047.

19. N. Saouti, N. Westerhof, P. E. Postmus, and A. Vonk-Noordegraaf, "The Arterial Load in Pulmonary Hypertension," *European Respiratory Review* 19 (2010): 197–203, https://doi.org/10.1183/09059180.00002210.

20. T. Kuehne, S. Yilmaz, P. Steendijk, et al., "Magnetic Resonance Imaging Analysis of Right Ventricular Pressure-Volume Loops," *Circulation* 110 (2004): 2010–2016, https://doi.org/10.1161/01.CIR.0000143138.02493.DD.

21. M. J. Richter, S. Hsu, A. Yogeswaran, et al., "Right Ventricular Pressure-Volume Loop Shape and Systolic Pressure Change in Pulmonary Hypertension," *American Journal of Physiology-Lung Cellular and Molecular Physiology* 320 (2021): L715–L725, https://doi.org/10.1152/ajplung.00583.2020.

22. A. Bellofiore and N. C. Chesler, "Methods for Measuring Right Ventricular Function and Hemodynamic Coupling With the Pulmonary Vasculature," *Annals of Biomedical Engineering* 41 (2013): 1384–1398, https://doi.org/10.1007/s10439-013-0752-3.

23. M. A. Quail, D. S. Knight, J. A. Steeden, et al., "Noninvasive Pulmonary Artery Wave Intensity Analysis in Pulmonary Hypertension," *American Journal of Physiology-Heart and Circulatory Physiology* 308 (2015): H1603–H1611, https://doi.org/10.1152/ajpheart.00480.2014.

24. M. U. Qureshi and N. A. Hill, "A Computational Study of Pressure Wave Reflections in the Pulmonary Arteries," *Journal of Mathematical Biology* 71 (2015): 1525–1549, https://doi.org/10.1007/s00285-015-0867-2.

25. S. A. van Wolferen, J. T. Marcus, N. Westerhof, et al., "Right Coronary Artery Flow Impairment in Patients With Pulmonary Hypertension," *European Heart Journal* 29 (2007): 120–127, https://doi.org/10.1093/eurheartj/ehm567.

26. H. Brooks, E. S. Kirk, P. S. Vokonas, C. W. Urschel, and E. H. Sonnenblick, "Performance of the Right Ventricle Under Stress: Relation to Right Coronary Flow," *Journal of Clinical Investigation* 50 (1971): 2176–2183, https://doi.org/10.1172/JCI106712.

27. A. Gómez, D. Bialostozky, A. Zajarias, et al., "Right Ventricular Ischemia in Patients With Primary Pulmonary Hypertension," *Journal of the American College of Cardiology* 38 (2001): 1137–1142, https://doi.org/10.1016/S0735-1097(01)01496-6.

28. A. Hamud, M. Brezins, A. Shturman, A. Abramovich, and R. Dragu, "Right Coronary Artery Diastolic Perfusion Pressure on Outcome of Patients With Left Heart Failure and Pulmonary Hypertension," *ESC Heart Failure* 8 (2021): 4086–4092, https://doi.org/10.1002/ehf2.13469.

29. J. Vogel-Claussen, J. Skrok, M. L. Shehata, et al., "Right and Left Ventricular Myocardial Perfusion Reserves Correlate With Right Ventricular Function and Pulmonary Hemodynamics in Patients With Pulmonary Arterial Hypertension," *Radiology* 258 (2011): 119–127, https://doi.org/10.1148/radiol.10100725.

30. S. Hungerford, K. Kearney, N. Song, et al., "Characteristic Changes to Pulsatile and Steady-State Load According to Pulmonary Hypertension Classification," *Physiological Reports* 11 (2023): e15662, https://doi.org/10.14814/phy2.15662.

31. V. Franco, "Right Ventricular Remodeling in Pulmonary Hypertension," *Heart Failure Clinics* 8 (2012): 403–412, https://doi.org/10.1016/j.hfc.2012.04.005.

32. P. R. Fourie, A. R. Coetzee, and C. T. Bolliger, "Pulmonary Artery Compliance: Its Role in Right Ventricular-Arterial Coupling," *Cardiovascular Research* 26 (1992): 839–844, https://doi.org/10.1093/cvr/26.9.839.

33. J. Sanz, A. García-Alvarez, L. Fernández-Friera, et al., "Right Ventriculo-arterial Coupling in Pulmonary Hypertension: A Magnetic Resonance Study - PubMed." *Heart (British Cardiac Society)* (2012). 98, https://doi.org/10.1136/heartjnl-2011-300462.

34. Z. A. Rako, N. Kremer, A. Yogeswaran, M. J. Richter, and K. Tello, "Adaptive Versus Maladaptive Right Ventricular Remodelling," *ESC Heart Failure* 10 (2023): 762–775, https://doi.org/10.1002/ehf2.14233.

35. H. J. Bogaard, K. Abe, A. Vonk Noordegraaf, and N. F. Voelkel, "The Right Ventricle Under Pressure," *Chest* 135 (2009): 794–804, https://doi.org/10.1378/chest.08-0492.

36. M. I. Burgess, N. Mogulkoc, R. J. Bright-Thomas, P. Bishop, J. J. Egan, and S. G. Ray, "Comparison of Echocardiographic Markers of Right Ventricular Function in Determining Prognosis in Chronic Pulmonary Disease," *Journal of the American Society of Echocardiography* 15 (2002): 633–639, https://doi.org/10.1067/mje.2002.118526.

37. S. Ghio, C. Klersy, G. Magrini, et al., "Prognostic Relevance of the Echocardiographic Assessment of Right Ventricular Function in Patients With Idiopathic Pulmonary Arterial Hypertension," *International Journal of Cardiology* 140 (2010): 272–278, https://doi.org/10.1016/j.ijcard.2008.11.051.

38. G. E. D'Alonzo, R. J. Barst, S. M. Ayres, et al., "Survival in Patients With Primary Pulmonary Hypertension," *Annals of Internal Medicine* 115 (1991): 343–349, https://doi.org/10.7326/0003-4819-115-5-343.

39. N. M. Fine, L. Chen, P. M. Bastiansen, et al., "Outcome Prediction by Quantitative Right Ventricular Function Assessment in 575 Subjects Evaluated for Pulmonary Hypertension," *Circulation: Cardiovascular Imaging* 6 (2013): 711–721, https://doi.org/10.1161/CIRCIMAGING.113.000640.

40. A. López-Candales, K. Dohi, N. Rajagopalan, et al., "Right Ventricular Dyssynchrony in Patients With Pulmonary Hypertension is Associated With Disease Severity and Functional Class," *Cardiovascular Ultrasound* 3 (2005): 23, https://doi.org/10.1186/1476-7120-3-23.

41. A. P. Kalogeropoulos, V. V. Georgiopoulou, S. Howell, et al., "Evaluation of Right Intraventricular Dyssynchrony by Two-Dimensional Strain Echocardiography in Patients With Pulmonary Arterial Hypertension," *Journal of the American Society of Echocardiography* 21 (2008): 1028–1034, https://doi.org/10.1016/j.echo.2008.05.005.

42. M. Murata, T. Tsugu, T. Kawakami, et al., "Right Ventricular Dyssynchrony Predicts Clinical Outcomes in Patients With Pulmonary Hypertension," *International Journal of Cardiology* 228 (2017): 912–918, https://doi.org/10.1016/j.ijcard.2016.11.244.

43. M. L. A. Haeck, U. Höke, N. A. Marsan, et al., "Impact of Right Ventricular Dyssynchrony on Left Ventricular Performance in Patients With Pulmonary Hypertension," *The International Journal of Cardiovascular Imaging* 30 (2014): 713–720, https://doi.org/10.1007/s10554-014-0384-1.

44. B. A. Maron, E. L. Brittain, E. Hess, et al., "Pulmonary Vascular Resistance and Clinical Outcomes in Patients With Pulmonary Hypertension: A Retrospective Cohort Study," *The Lancet Respiratory Medicine* 8 (2020): 873–884, https://doi.org/10.1016/S2213-2600(20)30317-9.

45. M. M. Hoeper, J. A. Barberà, R. N. Channick, et al., "Diagnosis, Assessment, and Treatment of Non-Pulmonary Arterial Hypertension Pulmonary Hypertension," *Journal of the American College of Cardiology* 54 (2009): S85–S96, https://doi.org/10.1016/j.jacc.2009.04.008.

46. M. C. van de Veerdonk, T. Kind, J. T. Marcus, et al., "Progressive Right Ventricular Dysfunction in Patients With Pulmonary Arterial Hypertension Responding to Therapy," *Journal of the American College of Cardiology* 58 (2011): 2511–2519, https://doi.org/10.1016/j.jacc.2011.06.068.

47. A. Macchia, R. Marchioli, G. Tognoni, et al., "Systematic Review of Trials Using Vasodilators in Pulmonary Arterial Hypertension: Why a New Approach is Needed," *American Heart Journal* 159 (2010): 245–257, https://doi.org/10.1016/j.ahj.2009.11.028.

48. A. Vonk-Noordegraaf, F. Haddad, K. M. Chin, et al., "Right Heart Adaptation to Pulmonary Arterial Hypertension," *Journal of the American College of Cardiology* 62 (2013): D22–D33, https://doi.org/10.1016/j.jacc.2013.10.027.

49. R.-S. Wang, S. Huang, S. W. Waldo, et al., "Elevated Pulmonary Arterial Compliance is Associated With Survival in Pulmonary Hypertension: Results From a Novel Network Medicine Analysis," *American Journal of Respiratory and Critical Care Medicine* 208 (2023): 312–321, https://doi.org/10.1164/rccm.202211-2097OC.

50. N. Al-Naamani, I. R. Preston, J. K. Paulus, N. S. Hill, and K. E. Roberts, "Pulmonary Arterial Capacitance is an Important Predictor of Mortality in Heart Failure With a Preserved Ejection Fraction," *JACC: Heart Failure* 3 (2015): 467–474, https://doi.org/10.1016/j.jchf.2015.01.013.

51. B. Boerrigter, G.-J. Mauritz, J. T. Marcus, et al., "Progressive Dilatation of the Main Pulmonary Artery is a Characteristic of Pulmonary Arterial Hypertension and is not Related to Changes in Pressure," *Chest* 138 (2010): 1395–1401, https://doi.org/10.1378/chest.10-0363.

52. J. Hurdman, R. Condliffe, C. A. Elliot, et al., "Aspire Registry: Assessing the Spectrum of Pulmonary Hypertension Identified at a Referral Centre," *European Respiratory Journal* 39 (2012): 945–955, https://doi.org/10.1183/09031936.00078411.

53. S. Mahapatra, R. A. Nishimura, P. Sorajja, S. Cha, and M. D. McGoon, "Relationship of Pulmonary Arterial Capacitance and Mortality in Idiopathic Pulmonary Arterial Hypertension," *Journal of the American College of Cardiology* 47 (2006): 799–803, https://doi.org/10.1016/j.jacc.2005.09.054.

54. D. M. Tabima, J. L. Philip, and N. C. Chesler, "Right Ventricular-Pulmonary Vascular Interactions," *Physiology* 32 (2017): 346–356, https://doi.org/10.1152/physiol.00040.2016.

55. D. Chemla, E. M. T. Lau, Y. Papelier, P. Attal, and P. Hervé, "Pulmonary Vascular Resistance and Compliance Relationship in Pulmonary Hypertension," *European Respiratory Journal* 46 (2015): 1178–1189, https://doi.org/10.1183/13993003.00741-2015.

56. C. Gerges, K. Vollmers, M. R. Pritzker, et al., "Pulmonary Artery Endovascular Device Compensates for Loss of Vascular Compliance in Pulmonary Arterial," *Journal of the American College of Cardiology* 76 (2020): 2284–2286, https://doi.org/10.1016/j.jacc.2020.08.080.

57. C. Gerges, K. Vollmers, N. Skoro-Sajer, et al., "Efficacy and Safety of the Aria Pulmonary Endovascular Device in Pulmonary Hypertension," *European Journal of Heart Failure* 26 (2024): 686–694, https://doi.org/10.1002/ejhf.3187.

58. F. Castagna, S. Viswanathan, G. Chalhoub, et al., "Predicting Hemodynamic Changes During Intra-Aortic Balloon Pump Support With a Longitudinal Evaluation," *ASAIO Journal* 69 (2023): 977–983, https://doi.org/10.1097/MAT.0000000000002014.

59. S. Scheidt, G. Wilner, H. Mueller, et al., "Intra-Aortic Balloon Counterpulsation in Cardiogenic Shock," *New England Journal of Medicine* 288 (1973): 979–984, https://doi.org/10.1056/NEJM197305102881901.

60. L. Baldetti, M. Pagnesi, M. Gramegna, et al., "Intra-Aortic Balloon Pumping in Acute Decompensated Heart Failure With Hypoperfusion: From Pathophysiology to Clinical Practice," *Circulation: Heart Failure* 14 (2021): e008527, https://doi.org/10.1161/CIRCHEARTFAILURE.121.008527.

61. H. Parissis, V. Graham, S. Lampridis, M. Lau, G. Hooks, and P. C. Mhandu, "IABP: History-Evolution-Pathophysiology-Indications: What We Need to Know," *Journal of Cardiothoracic Surgery* 11 (2016): 122, https://doi.org/10.1186/s13019-016-0513-0.

62. P. Bordachar, S. Lafitte, S. Reuter, et al., "Biventricular Pacing and Left Ventricular Pacing in Heart Failure," *Journal of Cardiovascular Electrophysiology* 15 (2004): 1342–1347, https://doi.org/10.1046/j.1540-8167.2004.04318.x.

63. J. B. Young, "Combined Cardiac Resynchronization and Implantable Cardioversion Defibrillation in Advanced Chronic Heart Failure," *Journal of the American Medical Association* 289 (2003): 2685, https://doi.org/10.1001/jama.289.20.2685.

64. D. P. S. Rogers, S. Marazia, A. W. Chow, et al., "Effect of Biventricular Pacing on Symptoms and Cardiac Remodelling in Patients With End-Stage Hypertrophic Cardiomyopathy," *European Journal of Heart Failure* 10 (2008): 507–513, https://doi.org/10.1016/j.ejheart.2008.03.006.

65. P. Steendijk, S. A. Tulner, J. J. Bax, et al., "Hemodynamic Effects of Long-Term Cardiac Resynchronization Therapy," *Circulation* 113 (2006): 1295–1304, https://doi.org/10.1161/CIRCULATIONAHA.105.540435.

66. S. Tian, J. J. Steenhorst, K. Heiden, et al., "Mechanosensing and Mechanotransduction in Pulmonary Hypertension," in *Vascular Mechanobiology in Physiology and Disease* Vol 8, ed. S. Tian, J. J. Steenhorst, K. van der Heiden, et al. (Springer, 2021), 299–318, https://doi.org/10.1007/978-3-030-63164-2_11.

67. A. Wang and D. Valdez-Jasso, "Cellular Mechanosignaling in Pulmonary Arterial Hypertension," *Biophysical Reviews* 13 (2021): 747–756, https://doi.org/10.1007/s12551-021-00828-3.

68. E. A. Mendiola, D. da Silva Gonçalves Bos, D. M. Leichter, et al., "Right Ventricular Architectural Remodeling and Functional Adaptation in Pulmonary Hypertension," *Circulation. Heart failure* 16 (2023): 009768, https://doi.org/10.1161/CIRCHEARTFAILURE.122.009768.

69. M. Li, D. E. Scott, R. Shandas, K. R. Stenmark, and W. Tan, "High Pulsatility Flow Induces Adhesion Molecule and Cytokine mRNA Expression in Distal Pulmonary Artery Endothelial Cells," *Annals of Biomedical Engineering* 37 (2009): 1082–1092, https://doi.org/10.1007/s10439-009-9684-3.

70. F. Liu, C. M. Haeger, P. B. Dieffenbach, et al., "Distal Vessel Stiffening is an Early and Pivotal Mechanobiological Regulator of Vascular Remodeling and Pulmonary Hypertension," *JCI Insight* 1 (2016): e86987, https://doi.org/10.1172/jci.insight.86987.

71. P. B. Dieffenbach, C. M. Haeger, A. M. F. Coronata, et al., "Arterial Stiffness Induces Remodeling Phenotypes in Pulmonary Artery Smooth Muscle Cells via YAP/TAZ-Mediated Repression of Cyclooxygenase-2," *American Journal of Physiology–Lung Cellular and Molecular Physiology* 313 (2017): L628–L647, https://doi.org/10.1152/ajplung.00173.2017.

72. P. B. Dieffenbach, M. Maracle, D. J. Tschumperlin, and L. E. Fredenburgh, "Mechanobiological Feedback in Pulmonary Vascular Disease," *Frontiers in Physiology* 9 (2018): e00951, https://doi.org/10.3389/fphys.2018.00951.

73. K. Abe, M. Shinoda, M. Tanaka, et al., "Haemodynamic Unloading Reverses Occlusive Vascular Lesions in Severe Pulmonary Hypertension," *Cardiovascular Research* 111 (2016): 16–25, https://doi.org/10.1093/cvr/cvw070.

74. T. Sarashina, K. Nakamura, S. Akagi, et al., "Reverse Right Ventricular Remodeling After Lung Transplantation in Patients With Pulmonary Arterial Hypertension Under Combination Therapy of Targeted Medical Drugs," *Circulation Journal* 81 (2017): 383–390, https://doi.org/10.1253/circj.CJ-16-0838.

75. M. Kasimir, "Reverse Cardiac Remodelling in Patients With Primary Pulmonary Hypertension After Isolated Lung Transplantation," *European Journal of Cardio-Thoracic Surgery* 26 (2004): 776–781, https://doi.org/10.1016/j.ejcts.2004.05.057.

76. A. Ntalianis, C. J. Kapelios, J. Kanakakis, et al., "Prolonged Intra-Aortic Balloon Pump Support in Biventricular Heart Failure Induces Right Ventricular Reverse Remodeling," *International Journal of Cardiology* 192 (2015): 3–8, https://doi.org/10.1016/j.ijcard.2015.05.014.

77. T. Saito, K. Toda, S. Miyagawa, et al., "Abstract 17964: Right Ventricular Reverse Remodeling During Long-Term Continuous-Flow Left Ventricular Assist Device Support in Patients With Dilated Cardiomyopathy," *Circulation* 130 (2014): 130, https://doi.org/10.1161/circ.130.suppl_2.17964.

78. T. Imamura, C. Juricek, T. Song, et al., "Improvement in Biventricular Cardiac Function After Ambulatory Counterpulsation," *Journal of Cardiac Failure* 25 (2019): 20–26, https://doi.org/10.1016/j.cardfail.2018.11.001.